Received: 1 July 2022 | Revised: 26 December 2022 | Accepted: 3 May 2023 | Published on: 14 May 2023

DOI: 10.1002/joc.8111

RESEARCH ARTICLE

International Journal of Climatology RMetS

Concurrent daytime and nighttime heatwaves in the late 21st century over the CORDEX-East Asia phase 2 domain using multi-GCM and multi-RCM chains

Young-Hyun Kim[1,2] | Joong-Bae Ahn[1] | Myoung-Seok Suh[3] | Dong-Hyun Cha[2] | Eun-Chul Chang[3] | Seung-Ki Min[4] | Young-Hwa Byun[5] | Jin-Uk Kim[5]

[1]Department of Atmospheric Sciences, Pusan National University, Busan, Korea

[2]School of Urban and Environmental Engineering, Ulsan National Institute of Science and Technology, Ulsan, Republic of Korea

[3]Department of Atmospheric Science, Kongju National University, Gongju, Republic of Korea

[4]Division of Environmental Science and Engineering, Pohang University of Science and Technology, Pohang, South Korea

[5]Climate Change Research Team, National Institute of Meteorological Sciences, Seogwipo, Korea

Correspondence

Joong-Bae Ahn, Department of Atmospheric Sciences, Pusan National University, Busan, Korea.
Email: jbahn@pusan.ac.kr

Funding information

Cooperative Research Program for Agriculture Science and Technology Development, Rural Development Administration, Republic of Korea, Grant/Award Number: PJ01475503

Abstract

The adverse impacts of extreme heat on human health when a concurrent daytime and nighttime heatwave (CDNHW) occurs are greater than when daytime or nighttime heatwaves occur individually, because of the reduced recovery time from heat exposure. This study projects increases in CDNHW over the whole of East Asia under two Representative Concentration Pathway scenarios (RCP2.6 and RCP8.5) and two Shared Socioeconomic Pathway scenarios (SSP1-2.6 and SSP5-8.5). The daily maximum and minimum temperatures, which are used to define a CDNHW, are calculated of 3-hourly temperatures of 25 km horizontal resolution produced by 12 general circulation model and regional climate model chains participating in the Coordinated Regional Climate Downscaling Experiment East Asia phase 2 project. In Historical simulation (1981–2005), occurrence period and occurrence rate of CDNHW from April to September area-averaged in East Asia are 10.9 days and 0.9%, respectively. In projections for the future (2071–2100), occurrence period and occurrence rate of CDNHW will be 3 weeks and 3.7% (RCP2.6), 2 months and 20.5% (RCP8.5), 2 months and 15.6% (SSP1-2.6), and 3 months and 45.7% (SSP5-8.5). In addition, it is expected that the CDNHW intensity will increase, and the spatial extent of CDNHW will be extended. Although a CDNHW lasting less than 3 days is the most common, the proportion of CDNHWs lasting more than 10 days, compared to the total CDNHW frequency, will increase to 1.2% (RCP2.6), 7.2% (RCP8.5), 6.1% (SSP1-2.6), and 17.3% (SSP5-8.5) from 0.2% (Historical). Both occurrence rate and intensity of CDNHW will increase to a relatively large extent in Indochina, East and West China, and India. If the current greenhouse gas emissions continue, East Asia will experience unprecedented heat stress because the frequency and intensity of CDNHWs, which rarely occur during present-day, will increase significantly over all regions by the end of the 21st century.

KEYWORDS
CMIP5, CMIP6, concurrent heatwaves, CORDEX-East Asia phase 2, daytime heatwaves, multi-GCM and multi-RCM chains, nighttime heatwaves, representative concentration pathways (RCPs), shared socioeconomic pathways (SSPs)

1 | INTRODUCTION

The consecutive occurrence of hot days and hot nights increases the adverse impacts of extreme heat on human health, because the recovery time from heat exposure is reduced (Fischer & Schar, 2010; Opitz-Stapleton et al., 2016; Wang, Chen, et al., 2020; Zhang et al., 2020). According to recent studies, the frequency of hot days and hot nights is increasing, and that trend will accelerate in East Asia, including South Korea (Choi & Lee, 2019; Hong et al., 2018; Im et al., 2017), China (Chen & Dong, 2019; Chen & Li, 2017; Ding et al., 2018; Guo et al., 2018; Hu & Sun, 2020; Li et al., 2017, 2018; Wang, Feng, et al., 2020; Wu et al., 2020; You et al., 2018; Zhang et al., 2020), Mongolia (Tong et al., 2019), India (Ahsan et al., 2022; Mukherjee & Mishra, 2018; Panda et al., 2014), Vietnam (Opitz-Stapleton et al., 2016), most regions of Asia (Dong et al., 2018), the Northern Hemisphere (Wang, Chen, et al., 2020), and globally (Zhu et al., 2021).

It is expected that heat stress will be exacerbated due to global warming, and it is especially necessary to analyse future changes in the concurrent daytime and nighttime heatwave (CDNHW), a phenomenon that extreme hot temperatures last from day to night. Many previous studies focused on future changes in hot days or hot nights separately (Ahsan et al., 2022; Guo et al., 2018; Hu & Sun, 2020; Im et al., 2017; Li et al., 2018; Opitz-Stapleton et al., 2016; Wang, Jiang, et al., 2019; Wu et al., 2020). Although most previous studies projected CDNHWs in specific regions or countries, the threshold for a CDNHW varied from study to study (Mukherjee & Mishra, 2018; Ullah et al., 2022 for India, Su & Dong, 2019, Wang, Feng, et al., 2020 for China). In other words, there has never been a comprehensive and integrated study that analysed CDNHWs over the whole of East Asia. Some studies showing future changes in CDNHWs by applying a united threshold to the northern hemisphere or on a global scale used data from the general circulation model (GCM) (Ma et al., 2022; Wang, Chen, et al., 2020; Zhu et al., 2021).However, those studies based on GCM projections have limited data resolution when it comes to simulating extreme events related to heat stress in East Asia with its complex topography.

In this study, we project a CDNHW by applying a united threshold that considers spatial and temporal climate characteristics over the whole of East Asia by the end of the 21st century by using 3-hourly temperature data with a 25 km horizontal resolution produced by 12 general circulation model–regional climate model (GCM-RCM) chains. The future simulations were based on two Representative Concentration Pathway (RCP) scenarios (RCP2.6 and RCP8.5) for GCMs from coupled model inter-comparison project phase 5 (CMIP5) and two Shared Socioeconomic Pathway (SSP) scenarios (SSP1-2.6 and SSP5-8.5) for GCMs from CMIP phase 6 (CMIP6).

2 | DATA AND ANALYSIS METHOD

2.1 | Model and observation data sets

This study utilizes the 3-hourly temperature data with a 25 km horizontal resolution from 12 GCM-RCM chains in the Coordinated Regional Climate Downscaling Experiment East Asia phase 2 (CORDEX-EA2) project (Figure 1). Eight GCM-RCM chains (HG2_CCLM,

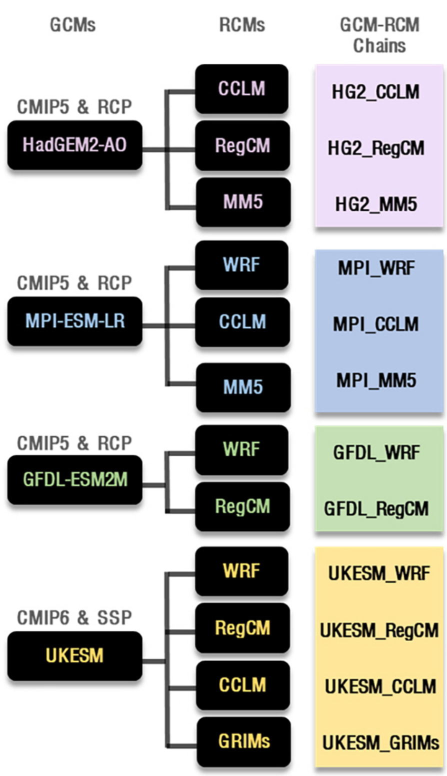

FIGURE 1 Twelve GCM-RCM chains. [Colour figure can be viewed at wileyonlinelibrary.com]

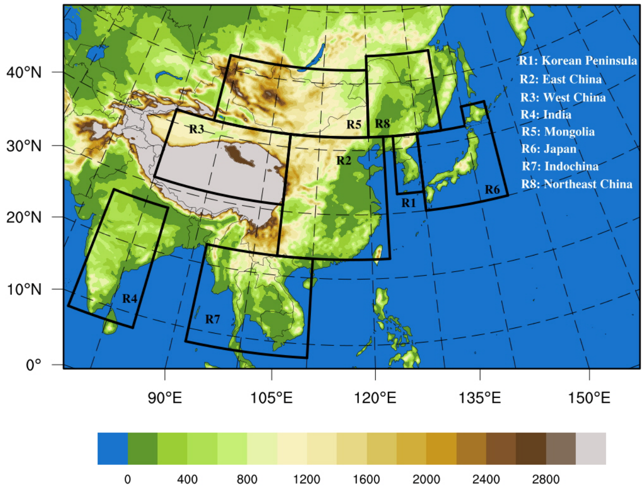

FIGURE 2 The CORDEX-East Asia phase 2 domain and topography (unit: m). Boxed areas indicate the eight sub-domains (R1–R8). [Colour figure can be viewed at wileyonlinelibrary.com]

HG2_RegCM, HG2_MM5, MPI_WRF, MPI_CCLM, MPI_MM5, GFDL_WRF, and GFDL_RegCM) are projections of three GCMs from CMIP5 under RCP2.6 and RCP8.5 scenarios that are dynamically downscaled using three or two RCMs. The other four GCM-RCM chains (UKESM_WRF, UKESM_CCLM, UKESM_RegCM, and UKESM_GRIM) are projections of one GCM from CMIP6 under SSP1-2.6 and SSP5-8.5 scenarios dynamically downscaled using four RCMs. The configurations of the 12 GCM-RCM chains are summarized in Table S1. The multi-model ensemble (ENS), which is the average of GCM-RCM chains with equal weighting, is mainly used to enhance the reliability of future climate projections compared to a single model. The averages for HG2_CCLM, HG2_RegCM, HG2_MM5, MPI_WRF, MPI_CCLM, MPI_MM5, GFDL_WRF, and GFDL_RegCM (UKESM_WRF, UKESM_CCLM, UKESM_GRIMs, and UKESM_RegCM) for Historical, RCP2.6, and RCP8.5 simulations (Historical, SSP1-2.6, and SSP5-8.5 simulations) are ENS_CMIP5_HIS, ENS_RCP26, and ENS_RCP85 (ENS_CMIP6_HIS, ENS_SSP126, and ENS_SSP585), respectively. The average of the 12 GCM-RCM chains for the Historical simulation is named ENS_ALL_HIS. The analysis results for the present climate show only ENS_ALL_HIS, even though a future change is calculated based on the differences between ENS_RCP26 or ENS_RCP85 (ENS_SSP126 or ENS_SSP585) and ENS_CMIP5_HIS (ENS_CMIP6_HIS).

The analysis period is 25 years for the Historical simulation (1981–2005) and 30 years for RCP and SSP simulations (2071–2100). The analysis domain is the whole CORDEX-EA2 domain (Figure 2) and ocean grid points are masked as missing values. In order to analyse the characteristics of a CDNHW in each region in East Asia with its various climate zones, the whole domain is divided into several sub-domains: the Korean Peninsula (R1, 33–42° N, 125–130° E), East China (R2, 23–42° N, 104–123° E), West China (R3, 31–42° N, 80–104° E), India (R4, 8–27° N, 74–84° E), Mongolia (R5, 42–52° N, 88–120° E), Japan (R6, 30–42° N, 130–145° E), Indochina (R7, 8–23° N, 92–110° E), and Northeast China (R8, 42–54° N, 120–135° E). The daily maximum and minimum temperatures, which are variables used to define a CDNHW, are calculated from the highest and lowest values among the 3-hourly temperature data. In Historical, RCP, and SSP simulations, the period in which the annual maximum values are high for both the daily maximum and minimum temperatures varied between mid-April and early September in all of East Asia. That period is July and August on the Korean Peninsula and in Northeast China, but is June to August in West China, East China, and Mongolia. It is May to June in India, from July to September in Japan, and from April to June in Indochina. Therefore, the heatwave period for all of East Asia is selected as April 1 to September 30 (Figure S1).

In order to evaluate the performance of the 12 GCM-RCM chains, ERA5 reanalysis data provided by the European Centre for Medium-Range Weather Forecasts is used. Gridded data from 12 GCM-RCM chains are converted to the ERA5 grid with 0.25° resolution using a simple inverse distance weighting method to compare model results with observations.

2.2 | Variance scaling

In order to reduce systematic bias in each model, the daily maximum and minimum temperatures are bias-corrected using variance scaling, which is a method to correct both mean and variance in temperatures (Teutschbein & Seibert, 2012). The observation data used for bias correction is the aforementioned ERA5 reanalysis data. In Equations (1)–(8) below, T_{obs} indicates daily maximum or minimum temperature in the observation data, while T_{contr} and T_{scen} indicate daily maximum or minimum temperature in Historical and RCP or SSP simulations, respectively. First, the mean of the Historical simulation is corrected by adding the difference between the long-term monthly mean observation data and the Historical simulation: $(\mu_m(T_{\text{obs}})-\mu_m(T_{\text{contr}}))$ as seen in Equation (1). Each mean for RCP or SSP simulations is also corrected by adding the term that is assumed to remain unvaried, even for a future climate, expressed in Equation (2).

$$T^{*1}_{\mathrm{contr}} = T_{\mathrm{contr}} + \mu_m(T_{\mathrm{obs}}) - \mu_m(T_{\mathrm{contr}}) \tag{1}$$

$$T^{*1}_{\mathrm{scen}} = T_{\mathrm{scen}} + \mu_m(T_{\mathrm{obs}}) - \mu_m(T_{\mathrm{contr}}) \tag{2}$$

Thereafter, the mean corrected historical simulation, T^{*1}_{contr}, and the RCP or SSP simulation, T^{*1}_{scen}, are shifted on a monthly basis to a zero mean:

$$T^{*2}_{\mathrm{contr}} = T^{*1}_{\mathrm{contr}} - \mu_m\left(T^{*1}_{\mathrm{contr}}\right) \tag{3}$$

$$T^{*2}_{\mathrm{scen}} = T^{*1}_{\mathrm{scen}} - \mu_m\left(T^{*1}_{\mathrm{scen}}\right) \tag{4}$$

Then, the variances of T^{*2}_{contr} and T^{*2}_{scen} are corrected based on the ratio of the standard deviation of T_{obs} to that of T^{*2}_{contr} $\left(\sigma_m(T_{\mathrm{obs}}) \text{ and } \sigma_m\left(T^{*2}_{\mathrm{contr}}\right)\right)$:

$$T^{*3}_{\mathrm{contr}} = T^{*2}_{\mathrm{contr}} \cdot \left[\frac{\sigma_m(T_{\mathrm{obs}})}{\sigma_m\left(T^{*2}_{\mathrm{contr}}\right)}\right] \tag{5}$$

$$T^{*3}_{\mathrm{scen}} = T^{*2}_{\mathrm{scen}} \cdot \left[\frac{\sigma_m(T_{\mathrm{obs}})}{\sigma_m\left(T^{*2}_{\mathrm{contr}}\right)}\right] \tag{6}$$

Finally, the mean- and variance-corrected Historical simulations and the RCP or SSP simulation, T^{*3}_{contr} and T^{*3}_{scen}, are shifted back using the value subtracted in Equations (3) and (4):

$$T^{*}_{\mathrm{contr}} = T^{*3}_{\mathrm{contr}} + \mu_m\left(T^{*1}_{\mathrm{contr}}\right) \tag{7}$$

$$T^{*}_{\mathrm{scen}} = T^{*3}_{\mathrm{scen}} + \mu_m\left(T^{*1}_{\mathrm{scen}}\right) \tag{8}$$

2.3 | Definition of CDNHW

In order to analyse a CDNHW in East Asia with various climate zones, the threshold of a heatwave considering spatial and temporal climate characteristics is needed. Therefore, the daily thresholds of daytime and nighttime heatwaves are defined as the 90th percentile of the daily maximum and minimum temperatures, centred on a 31-day window (i.e., 15 days before and after a Julian day) for the reference period (1981–2005), as referred to in Russo et al. (2015). Daytime and nighttime heatwaves are defined as a day where the daily maximum and minimum temperatures exceed the daily thresholds for daytime and nighttime heatwaves, respectively. The daily intensities of daytime and nighttime heatwaves are defined as follows (Russo et al., 2015):

$$INT\_DHW = \begin{cases} \dfrac{\mathrm{Tmax} - \mathrm{Tmax}_{25y25p}}{Tmax_{25y75p} - Tmax_{30y25p}} & (\mathrm{Tmax} > \mathrm{Tmax}_{25y25p}) \\ 0 & (\mathrm{Tmax} \leq \mathrm{Tmax}_{25y25p}) \end{cases} \tag{9}$$

$$INT\_NHW = \begin{cases} \dfrac{\mathrm{Tmin} - \mathrm{Tmin}_{25y25p}}{\mathrm{Tmin}_{25y75p} - \mathrm{Tmin}_{25y25p}} & (\mathrm{Tmin} > \mathrm{Tmin}_{25y25p}) \\ 0 & (\mathrm{Tmin} \leq \mathrm{Tmin}_{25y25p}) \end{cases} \tag{10}$$

In Equation (9), Tmax is the daily maximum temperature on day when a daytime heatwave occurs, while Tmax_{25y25p} and Tmax_{25y75p} are the 25th and 75th percentiles, respectively, for annual maximum values from daily maximum temperatures during the reference period. In Equation (10), Tmin is the daily minimum temperature on day when a nighttime heatwave occurs, while Tmin_{25y25p} and Tmin_{25y75p} are the 25th and 75th percentiles, respectively, for annual maximum values from daily minimum temperatures during the reference period. When INT_DHW is greater than 0 and INT_NHW is less than 0, it is defined as an independent daytime heatwave (IDHW), but when INT_DHW is less than 0 and INT_NHW is greater than 0, it is an independent nighttime heatwave (INHW). When both INT_DHW and INT_NHW are greater than 0, it is a CDNHW. The daily intensity of a CDNHW (INT_CDNHW) is defined as the sum of INT_DHW and INT_NHW on the day the CDNHW occurs. A day with the daily maximum or minimum temperature is higher than daily threshold of daytime or nighttime

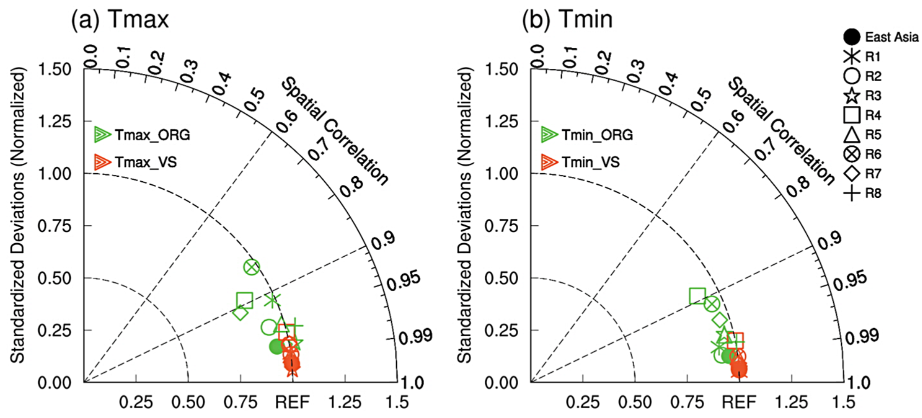

FIGURE 3 Taylor diagrams of the 25-year (1981–2005) mean (a) daily maximum temperature (Tmax) and (b) daily minimum temperature (Tmin) during the heatwave period in East Asia derived from ENS_ALL_HIS. Radial axes show the temporal standard deviation of ENS_ALL_HIS normalized with ERA5, and the arcs denote the spatial correlation coefficients between ENS_ALL_HIS and ERA5. The REF point (1.0) denotes where ENS_ALL_HIS exactly agrees with ERA5. In the legend, _ORG and _VS, respectively, indicate non-bias corrected and bias-corrected Tmax or Tmin. [Colour figure can be viewed at wileyonlinelibrary.com]

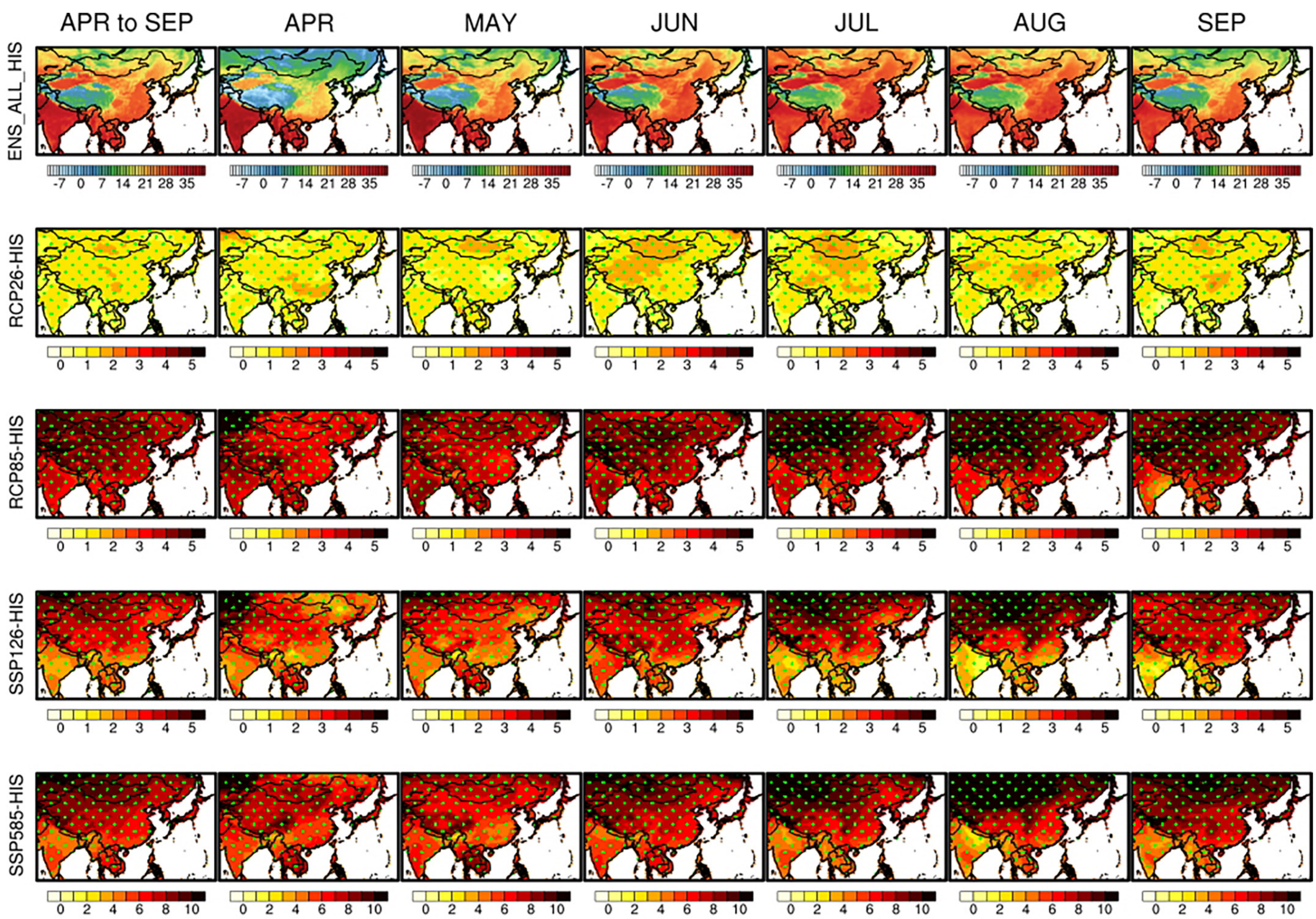

FIGURE 4 Spatial distributions of monthly mean daily maximum temperatures during the heatwave period from April to September in East Asia derived from (top) ENS_ALL_HIS, and the future changes derived from (second from the top to the bottom) ENS_RCP26, ENS_RCP85, ENS_SSP126, and ENS_SSP585 (unit: °C). The grid points where the difference is significant at the 95% confidence level based on the Student's *t*-test are marked with green dots. [Colour figure can be viewed at wileyonlinelibrary.com]

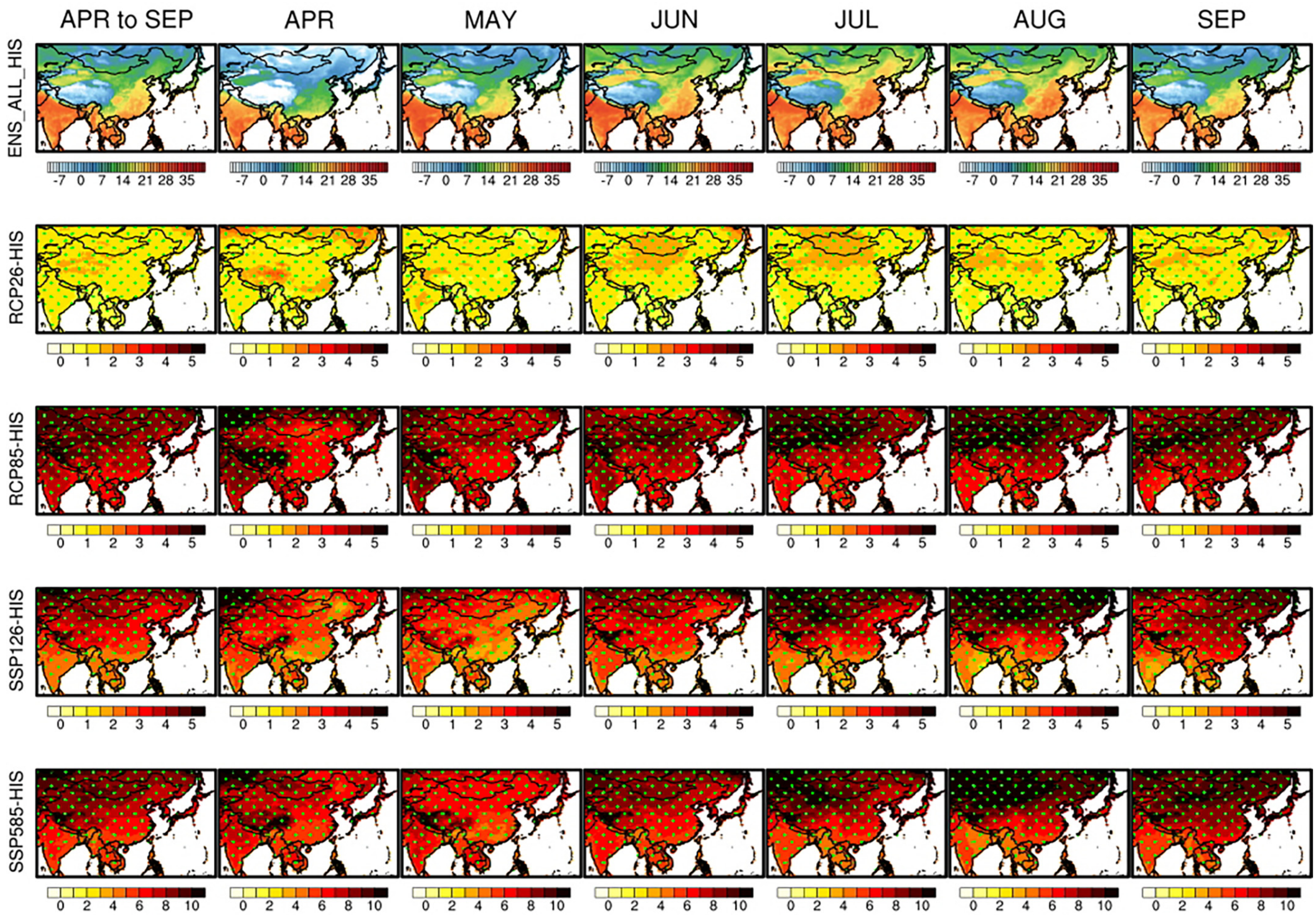

FIGURE 5 Same as Figure 4 but shows daily minimum temperatures. [Colour figure can be viewed at wileyonlinelibrary.com]

heatwave, although daily intensity is zero, is considered as a hot day or hot night, not as a heatwave day.

3 | RESULTS

First, the performance of ENS_ALL_HIS in simulating the daily maximum and minimum temperatures used to define a CDNHW is evaluated over the eight sub-domains. Figure 3 presents Taylor diagrams that show the temporal standard deviations for ENS_ALL_HIS normalized with ERA5 (NSD), and the spatial correlation coefficients (SCCs) between ENS_ALL_HIS and ERA5. The closer to the point marked REF (1.0), the more similar the performance of ENS_ALL_HIS to ERA5. The SCC and NSD for daily maximum temperatures derived from ENS_ALL_HIS before bias correction (Tmax_ORG) appear within the ranges 0.82–0.98 and 0.82–1.05, respectively, and those for the daily minimum temperatures derived from ENS_ALL_HIS before bias correction (Tmin_ORG) appear within the ranges 0.89–0.99 and 0.90–1.00, respectively. This means simulated daily maximum and minimum temperatures in ENS_ALL_HIS are similar to those of ERA5 in East Asia, although there are some variations depending on the region. The SCC for corrected daily maximum and minimum temperatures derived from ENS_ALL_HIS via the variance scaling method (Tmax_VS and Tmin_VS) appear within the ranges 0.97–1.00 and 0.98–1.00, respectively. Both NSDs for Tmax_VS and Tmin_VS are close to 1.0. Likewise, in 12 GCM-RCM chains, simulated daily maximum and minimum temperatures are also similar to those of ERA5 in East Asia and Tmax_VS and Tmin_VS are closer to the REF than Tmax_ORG and Tmin_ORG (Figure S2). In addition, through the probability distribution functions (Figure S3), we can see that the distribution ranges and shapes for Tmax_VS and Tmin_VS are more similar to those of ERA5 than Tmax_ORG and Tmin_ORG. Hence, CDNHWs were analysed using Tmax_VS and Tmin_VS in this study.

We investigate the temporal and spatial characteristics of daily maximum (Tmax) and minimum temperatures (Tmin) (Figures 4 and 5). In ENS_ALL_HIS, the Tmax and Tmin are the highest from April to June for India and Indochina; and in July or August for the

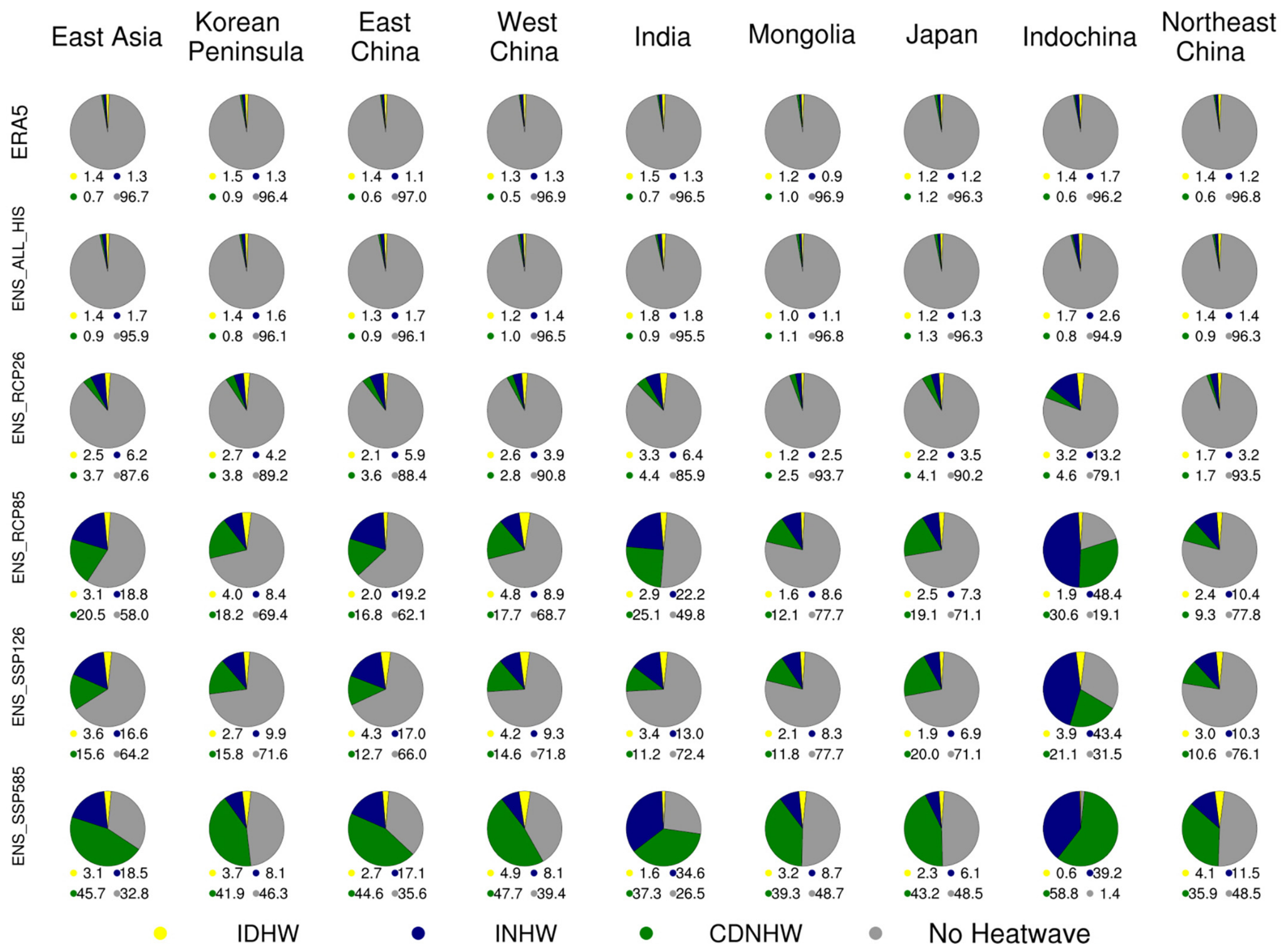

FIGURE 6 Pie charts showing independent daytime heatwave (IDHW), independent nighttime heatwave (INHW), and concurrent daytime and nighttime heatwave (CDNHW) occurrence rates during the heatwave periods over all of East Asia and the eight sub-regions, derived from (top row) ERA5, and (subsequently from top down) ENS_ALL_HIS, ENS_RCP26, ENS_RCP85, ENS_SSP126, and ENS_SSP585 (unit: %). [Colour figure can be viewed at wileyonlinelibrary.com]

Korean Peninsula, China, Mongolian, and Japan. In India and Indochina, the Tmax and Tmin are higher than other regions, while the monthly variability of those are relatively small (Figure S4). Figure S5 shows the spatial distributions of mean Tmax and Tmin during the heatwave period in East Asia from April to September derived from ERA5, ENS_CMIP5_HIS, and ENS_CMIP6_HIS, as well as the bias compared with ERA5. The magnitude of bias for mean Tmax and Tmin derived from ENS_CMIP5_HIS is smaller than that derived from ENS_CMIP6_HIS, which may be because ENS_CMIP6_HIS is forced by only one GCM, while ENS_CMIP5_HIS is forced by three GCMs. However, the difference between ENS_CMIP5_HIS and ENS_CMIP6_HIS is negligible over East Asia, except for the mean Tmax in India. These results indicate that ENS_SSP126 and ENS_SSP585 can help to confirm that future projections of heatwaves under SSP126 and SSP585 scenarios support those under RCP2.6 and RCP8.5 scenarios. The temporal and spatial characteristics of a daytime and nighttime heatwave threshold is similar to the daily maximum and daily minimum temperatures (Figure S6).

In ENS_RCP26, ENS_RCP85, ENS_SSP126, and ENS_SSP585, the Tmax and Tmin increase in all regions of East Asia, especially, more increase in high-latitude region and more increase during the period when temperatures are already high in ENS_ALL_HIS. In addition, the Tmin increase more than Tmax in East Asia expect for East China and Indochina. The average of Tmax/Tmin during the period from April to September increase from 22.5°C/13.9°C (ENS_ALL_HIS) to 23.6°C/15.1°C (ENS_RCP26), 26.3°C/17.7°C (ENS_RCP85), 25.6°C/17.0°C (ENS_SSP126), and 29.5°C/21.0°C (ENS_SSP585) in East Asia. Therefore, the increases are large in the following order: ENS_SSP585, ENS_RCP85, ENS_SSP126, and ENS_RCP26. SSP5-8.5 and RCP8.5 (SSP1-2.6 and RCP2.6) scenarios represent the high-emission (low-emissions) scenarios with the same radiative forcing of 8.5 W/m^2 (2.6 W/m^2) by 2100, but the CO_2 emissions at the end of the 21st century in SSP5-8.5 (SSP1-2.6) scenario is approximately 21.0% (6.0%) higher than that in RCP8.5 (RCP2.6) scenario. Therefore, the Tmax and Tmin under SSP scenarios are higher than those under corresponding RCP scenarios.

Future changes in IDHWs, INHWs, and CDNHWs due to the increase in daily maximum and minimum temperatures were analysed. Figure 6 presents pie charts showing the occurrence rates for IDHWs, INHWs, and CDNHWs during the heatwave period in East Asia (OR_IDHW, OR_INHW, and OR_CDNHW). In ERA5, OR_IDHW, OR_INHW, and OR_CDNHW appear within the ranges 1.2%–1.5%, 0.9%–1.7%, and 0.5%–1.2% in the eight sub-regions, which means that CDNHWs occur rarely than INHW and IDHW. Although ENS_ALL_HIS tends to overestimate or underestimate OR_IDHW, OR_INHW, and OR_CDNHW, depending on the sub-region, the absolute values in the bias of those area averages in East Asia are very small (0.1%, 0.5%, and 0.3%, respectively). This means OR_IDHW, OR_INHW, and OR_CDNHW derived from ENS_ALL_HIS and ERA5 are very similar. In ENS_RCP26, ENS_RCP85, ENS_SSP126, and ENS_SSP585, OR_IDHW, OR_INHW, and OR_CDNHW increase in all regions of East Asia. In addition, the regional differences in OR_IDHW, OR_INHW, and OR_CDNHW are large compared to ENS_ALL_HIS because the degree of the increase vary depending on the region. In the current climate, the occurrence rate of a CDNHW area-averaged in East Asia is 0.9%, which is lower than for IDHWs (1.4%) and INHWs (1.6%). In the future, the occurrence rates of CDNHWs area-averaged in East Asia will increase to 3.7% (RCP2.6), to 20.5% (RCP8.5), to 15.6% (SSP1-2.6), and to 45.7% (SSP5-8.5), and will be higher in Indochina than in other regions. Even, CDNHW more occurs than IDHW and INHW in Mongolia and Japan (RCP2.6), on the Korean Peninsula,

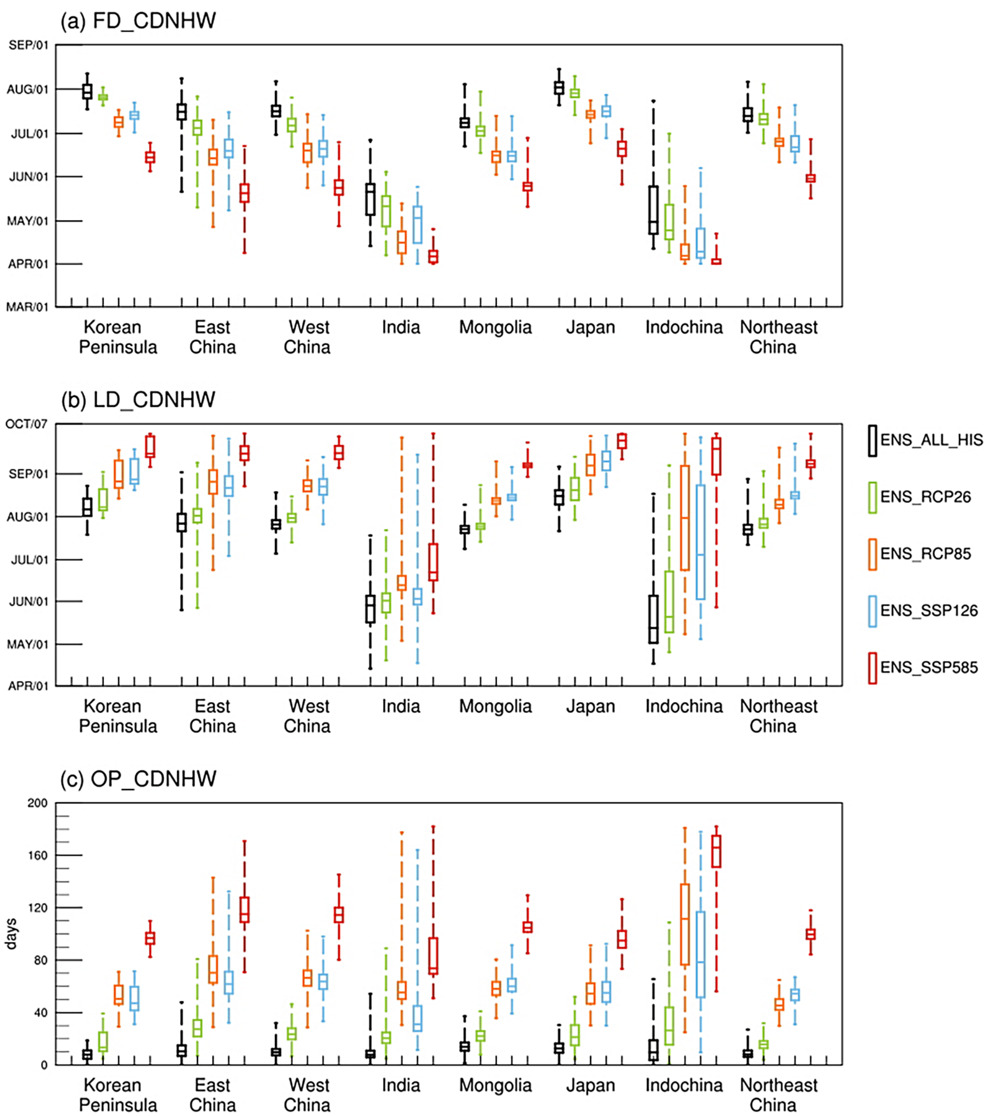

FIGURE 7 Box plots showing the climatology of the (a) first date and (b) last date when CDNHWs occur (FD_CDNHW and LD_CDNHW) and (c) the climatology of the CDNHW occurrence period (OP_CDNHW) for grids in the eight sub-domains. Each box denotes the range from the 25th percentile to the 75th percentile. The line in the middle of the box denotes the median. The upper and lower whiskers indicate maximum and minimum values. [Colour figure can be viewed at wileyonlinelibrary.com]

and in East and West China, India, Mongolia, and Japan (RCP8.5), on the Korean Peninsula, and in West China, Mongolia, Japan, and Northeast China (SSP1-2.6), and in all regions of East Asia (SSP5-8.5).

In order to examine the characteristics of a CDNHW, first, the period in which the CDNHW mainly occurs in each sub-domain is analysed. Box plots presented in Figure 7 show the climatology of the Julian day when CDNHW occurs first and last (first date and last date of CDNHW) and the climatology of CDNHW occurrence period, which is calculated as the difference between last date and first date of CDNHW, for grids in the eight sub-domain. In ENS_ALL_HIS, CDNHWs mainly occurs from late July to mid-August on the Korean Peninsula, from mid-July to early August in East and West China, from early-May to early June in India, from early to late July in Mongolia, from late July to mid-August in Japan, from late April to early June in Indochina, and from mid to late July in Northeast China. The area-averaged occurrence period of CDNHW in East Asia is about 10.9 days, which is relatively long in East China, Mongolia, Japan, and Indochina. In ENS_RCP26, ENS_RCP85, ENS_SSP126, and ENS_SSP585, the first date of CDNHW is earlier and last date of CDNHW is later than in ENS_ALL_HIS, respectively (Tables S2 and S3). Therefore, the occurrence period of CDNHW area-averaged in East Asia extends to about 23.2 days (RCP2.6), 66.0 days (RCP8.5), 59.3 days (SSP1-2.6), and 110.2 days (SSP5-8.5). In other words, CDNHWs occur even when CDNHWs do not usually occur in ENS_ALL_HIS. The occurrence period is relatively longer in East and West China, Mongolia, and Indochina (RCP2.6), in East and West China and Indochina (RCP8.5 and SSP5-8.5) and in East and West China, Mongolia, and Indochina (SSP1-2.6), compared to other regions.

Figure 8 presents the frequency of CDNHWs of various durations. In ENS_ALL_HIS (Figure 8a), the duration of a CDNHW is mostly from 1 to 3 days in East Asia. Although the frequency of all CDNHWs is high in Mongolia and Japan, CDNHWs lasting more than 4 days occur more in India and Japan than other regions. In ENS_RCP26, ENS_RCP85, ENS_SSP126, and ENS_SSP585, the frequency of all CDNHWs increases, with a CDNHW lasting fewer than 3 days being the most common, as seen in ENS_ALL_HIS. In particular, long-lasting CDNHWs, which rarely occurs in ENS_ALL_HIS, occur. In

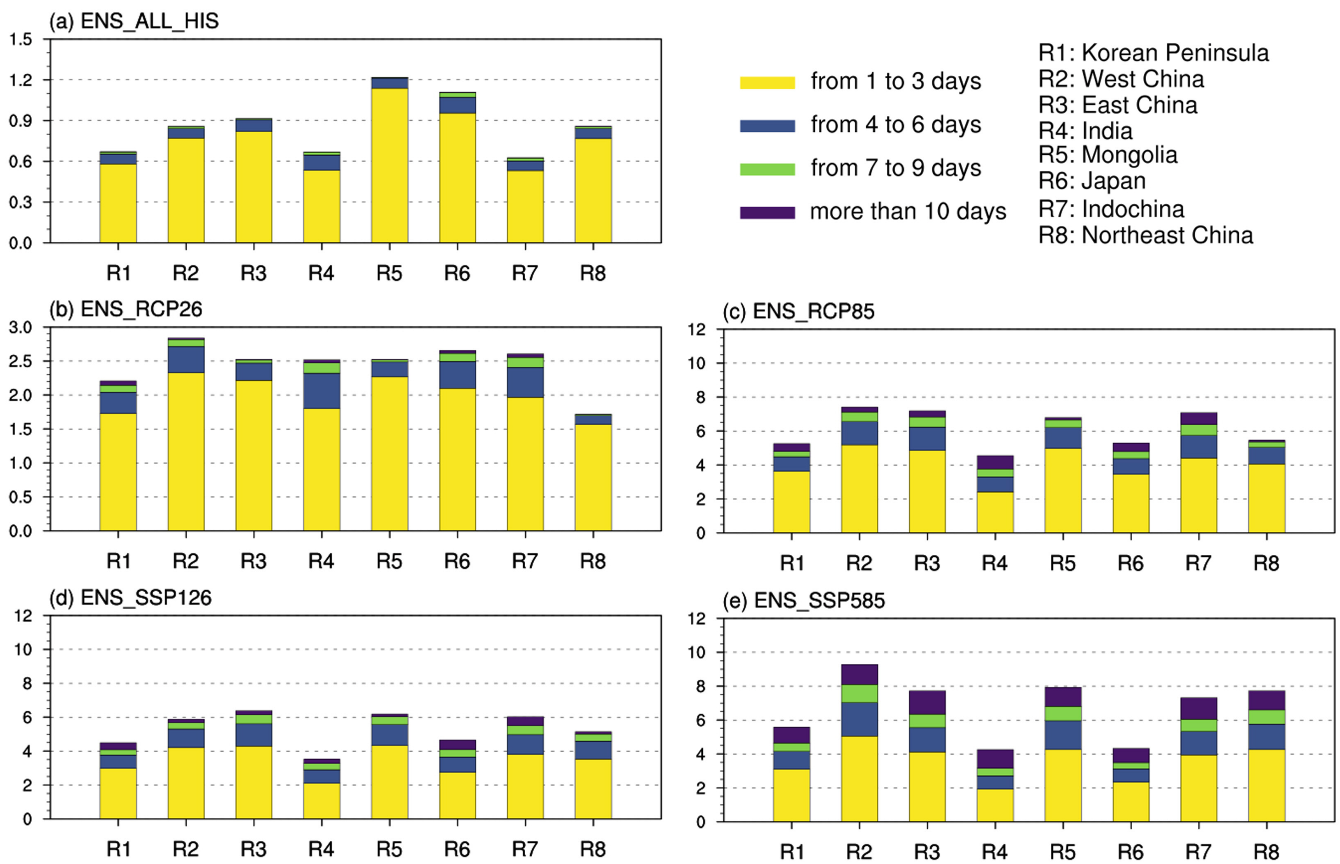

FIGURE 8 Frequency of concurrent daytime and nighttime heatwaves (CDNHWs) of various durations over the eight sub-regions for (a) ENS_ALL_HIS, (b) ENS_RCP26, (c) ENS_RCP85, (d) ENS_SSP126, and (e) ENS_SSP585. [Colour figure can be viewed at wileyonlinelibrary.com]

ENS_RCP26 (Figure 8b), CDNHWs lasting more than 7 days occur on the Korean Peninsula, and in East China, India, Japan, and Indochina. In ENS_RCP85 and ENS_SSP126 (Figure 8c,d), CDNHWs lasting more than 7 days occur in all regions of East Asia, and those lasting more than 10 days occur in most regions of East Asia except for Mongolia and Northeast China. In ENS_ SSP585 (Figure 8e), CDNHWs lasting more than 10 days occurs in all regions of East Asia. Therefore, the proportion of CDNHWs lasting more than 10 days, compared to the frequency of all CDNHWs, in East Asia will increase to 1.2% (RCP2.6), 7.2% (RCP8.5), 6.1% (SSP1-2.6), and 17.3% (SSP5-8.5) from 0.2% (Historical). These long-lasting CDNHWs will occur more frequently in India and Indochina under RCP2.6 and RCP8.5 scenarios, in Japan and Indochina under SSP1-2.6 scenario, and in India and Japan under SSP5-8.5 scenario. Among the high-emission scenarios, CDNHW lasting more than 10 days is three times more frequent in SSP5-8.5 scenario than RCP8.5 scenario.

Finally, we investigated future changes in the intensity of CDNHWs due to increases in the occurrence periods and the number of days they last. Figure 9 and Figure S7 show the spatial distributions for accumulated intensity of CDNHWs derived from ENS_ALL_HIS, ENS_RCP26, ENS_RCP85, ENS_SSP126, and ENS_SSP585 and their differences. The spatial extent of CDNHW, which is calculated as a percentage of CDNHW area to the total sub-domain area, is shown in Figure S8. In ENS_ALL_HIS, the accumulated intensity of CDNHW from April to September is relatively high in West China (except for the Tibetan Plateau), in some regions of East China, India, and in Thailand and Cambodia in Indochina. The period when intensity of CDNHW is the highest over a broad area is May in India and Indochina, and July or August on the Korean Peninsula, in China, in Mongolia, and in Japan.

In ENS_RCP26, ENS_RCP85, ENS_SSP126, and ENS_SSP585, not only the intensity of CDNHW more increases, but also the spatial and temporal extent of the CDNHW is more expanded. The intensity of CDNHW increases in all regions of East Asia and that increases more in East China, West China, India and in Indochina,

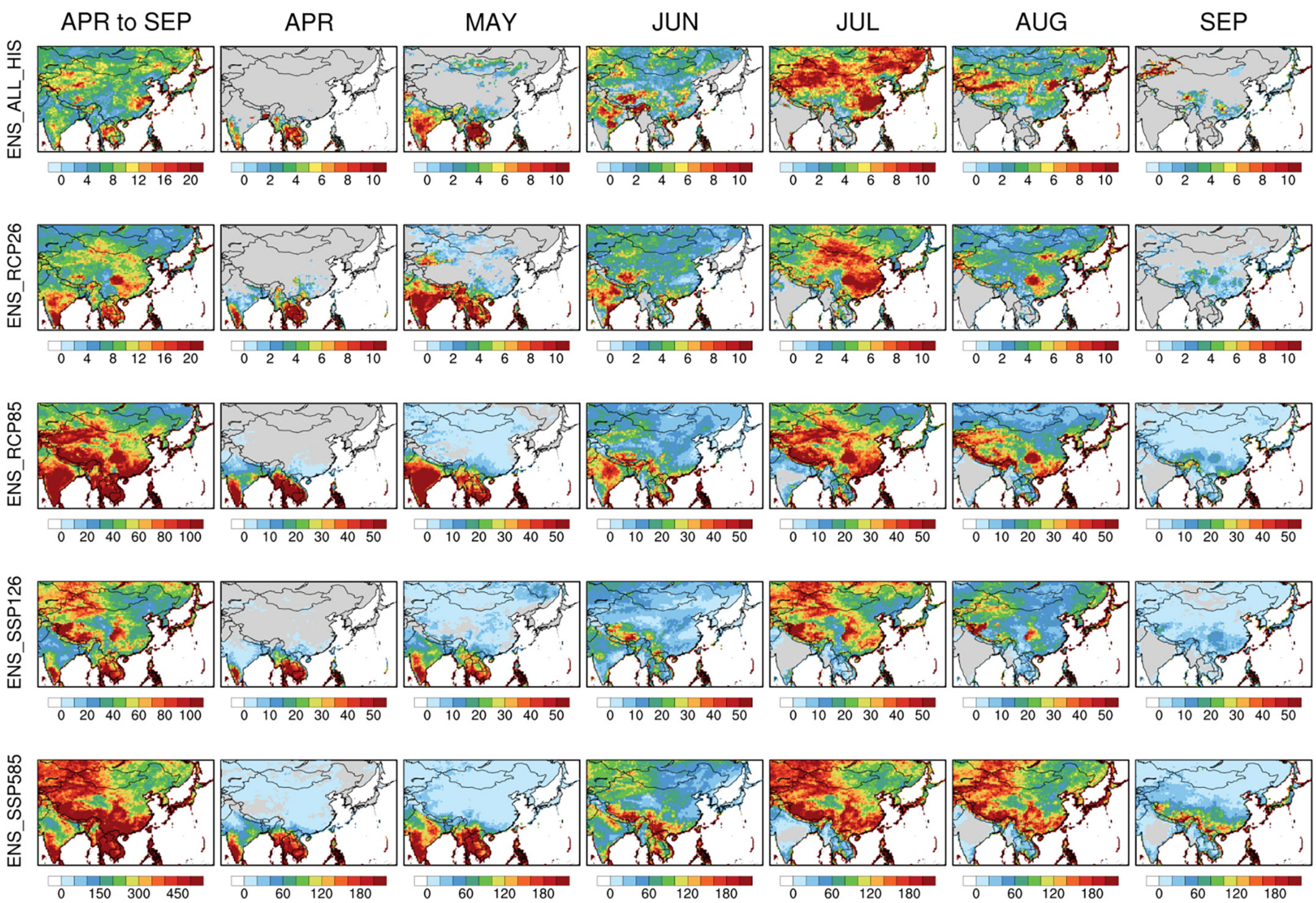

FIGURE 9 Spatial distributions for monthly accumulated intensity of concurrent daytime and nighttime heatwaves (CDNHWs) during the heatwave period in East Asia from April to September for (top to bottom) ENS_ALL_HIS, ENS_RCP26, ENS_RCP85, ENS_SSP126, and ENS_SSP585. [Colour figure can be viewed at wileyonlinelibrary.com]

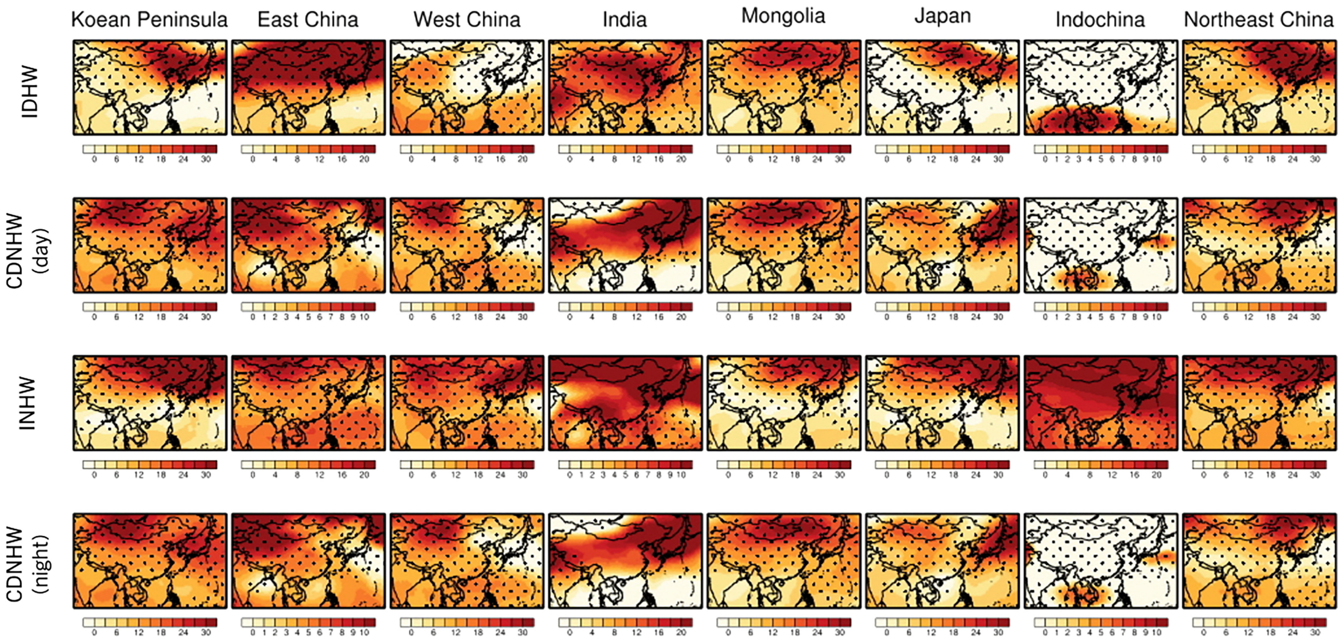

FIGURE 10 Composites of geopotential height at 500 hPa anomalies during daytime for IDHWs (top row) and CDNHWs (second row), and during nighttime for INHWs (third row) and CDNHWs (bottom row) over eight sub-regions (unit: m) in historical simulation. The grid points where the anomaly is significant at the 95% confidence level based on the Student's *t*-test are marked with black dots. [Colour figure can be viewed at wileyonlinelibrary.com]

where the already more affected by CDNHW in ENS_ALL_HIS. While, the intensity of CDNHW derived from ENS_RCP26 decrease in the eastern part of East China, the western part of West China, and Northeast China. The increase in the intensities of CDNHWs is larger in the order of SSP5-8.5, RCP8.5, SSP1-2.6, and RCP2.6 scenarios. In particular, the increase is four times stronger under SSP5-8.5 scenario than RCP8.5 scenario. In addition, CDNHW occurs even in the period when the CDNHW rarely occurs in ENS_ALL_HIS (in May, June, and September on the Korean Peninsula, in April in East China, in April and May in West China, from July to September in India, in April and September in Mongolia, from April to June in Japan, in September in Indochina, and in April, May, and September in Northeast China).

4 | DISCUSSION AND CONCLUSION

The adverse effects of extreme heat are expected to increase due to global warming. In particular, CDNHWs will have negative impacts not only on ecosystems and human health, but across industries in all countries. Although quantitatively analysing future changes in CDNHWs (as well as daytime or nighttime heatwaves) is important, few studies have analysed future changes in CDNHWs over East Asia. In this study, CDNHWs over the whole of East Asia by the end of the 21st century (2071–2100) are projected under RCP2.6, RCP8.5, SSP1-2.6, and SSP5-8.5 scenarios using 3-hourly temperature data with a 25 km horizontal resolution produced by 12 GCM-RCM chains participating in the CORDEX-EA2 project.

To evaluate the performance of GCM-RCM chains in simulating daily maximum and minimum temperatures, NSD, SCC, and probability distribution functions were examined. As a result, the temporal and spatial climate characteristics of bias-corrected daily maximum and minimum temperatures under the variance scaling method were more similar to those of ERA5 than daily maximum and minimum temperatures before bias correction. In Historical simulation, the occurrence rate for CDNHWs from April to September (area-averaged in East Asia) is 0.9%, which is very low in all regions of East Asia. A CDNHW mainly occurs from July to August on the Korean Peninsula, in China, in Mongolia, and in Japan, and occurs from April to June in India and Indochina. The occurrence period for CDHNWs from first to last onset is about 1–2 weeks, and the duration of a CDNHW is usually less than 3 days. The period when the intensity of a CDNHW is the highest and when it covers the widest area is in July or August on the Korean Peninsula, in China, in Mongolia, and in Japan, and is in May for India and Indochina. The accumulated intensity of a CDNHW from April to September is higher in West

China, except for the Tibetan Plateau, and in East China, India, as well as Thailand and Cambodia in Indochina, compared to other regions.

By the end of the 21st century, the occurrence period for CDHNWs will be extended to 3 weeks (RCP2.6), to 2 months (RCP8.5 and SSP1-2.6), and to 3 months (SSP5-8.5), and the occurrence rates for CDNHWs will increase to 3.7% (RCP2.6), 20.5% (RCP8.5), 15.6% (SSP1-2.6), and 45.7% (SSP5-8.5), as the daily maximum and minimum temperatures from April to September will increase in all regions of East Asia. Therefore, it is expected that the intensity of CDNHWs will increase, and the spatial extent of CDNHW will be expanded. The period when the intensity of a CDNHW is the highest and when it covers the widest area will be expected to be the same period as in Historical simulation. CDNHWs lasting less than 3 days are most common, but the frequency of CDNHWs lasting more than 10 days will increase significantly. The occurrence period and duration of CDNHWs will be longest and occurrence rate and intensity of CDNHWs will be highest in Indochina, and those are longer or higher in East China, West China, and India, compared to other regions. More frequent, intense, and prolonged CDNHWs occur over a broad area in high-emission scenarios, particularly in SSP5-8.5 scenario, because future warming in East Asia is more pronounced under SSP scenarios than under corresponding RCP scenarios.

The physical or dynamical mechanisms responsible for the increase in intensity and frequency of CDNHWs in each region of East Asia should be explored in-depth in further study. Recently, many study attach the attention to CDNHWs, but underlying mechanism of CDNHWs remains unclear. Very few studies show that the persistent anticyclonic circulation is mainly associated with CDNHWs in East Asia regions (Li et al., 2021; Luo et al., 2022 for China, Wang et al., 2020 in Northern hemisphere). The anomalous anticyclone contributes to surface warming through adiabatic heating, additional solar radiation absorption, and offsetting the nighttime radiative cooling (Choi & Lee, 2019; Hong et al., 2018; Im et al., 2019; Kim et al., 2019; Lee & Lee, 2016; Noh et al., 2021; Seo et al., 2021; Yoon et al., 2020; Yoon et al., 2021 for Korean Peninsula, Freychet et al., 2017; Hong et al., 2020; Luo & Lau 2017; Park et al., 2012; Wang, Hui, et al., 2019; Wang, Jiang, et al., 2019 for China, Joshi et al., 2020; Ratnam et al., 2016; Rohini et al., 2016; Sandeep & Prasad, 2018 for India, Erdenebat & Sato, 2016 for Mongolia, Nishi et al., 2022; Noh et al., 2021 for Japan, Luo & Lao, 2018, for Indochina Peninsula). We carried out the composite analysis of the daytime and nighttime geopotential height at 500 hPa (Z500) anomalies for CDNHW events using 6-hourly Z500 data. Considering local time, Z500 at 06 UTC and 18 UTC were used to composite mean for daytime and nighttime hour, respectively. Figures S9 and S10 show that the positive Z500 anomalies persist day and night over the regions with CDNHW events in Historical simulation. In RCP and SSP scenarios, the magnitude of daytime and nighttime Z500 anomaly against reference period climatology increases, which may be one of the reasons for increase in CDNHWs.

Recently, the CDNHWs are receiving scientific attention, but the underlying mechanism related to that has been poorly understood. Very a few studies show that the persistent anticyclonic circulation is mainly associated with CDNHWs in East Asia regions (Li et al., 2021; Luo et al., 2022 for China, Wang et al., 2021 in Northern hemisphere). In order to understand the underlying mechanism associated with CDNHW in East Asia, first of all, we carried out the composite analysis of the daytime (06UTC) and nighttime (18UTC) geopotential height at 500 hPa (Z500) anomalies for CDNHW events. Figure 10 shows the composites of daytime or nighttime Z500 anomalies for each of IDHW, INHW, and CDNHW in Historical simulation. It is founded that positive Z500 anomalies is dominant during the day and night when IDHW and INHW occurs, and that persist day and night when CDNHW occurs over each sub-region. In general, under the anomalous anticyclone conditions, adiabatic heating due to sinking motion and additional solar radiation absorption due to reduction of cloud cover contribute to surface warming during the daytime. In addition, warm advection caused by anomalous wind, and, the reduction of nighttime radiative cooling due to anomalous moisture advection, particularly in coastal areas as well as the adiabatic heating elevates surface temperature during the night (Choi & Lee, 2019; Hong et al., 2018; Im et al., 2019; Kim et al., 2019; Lee & Lee, 2016; Noh et al., 2021; Seo et al., 2021; Yoon et al., 2020, 2021 for Korean Peninsula, Freychet et al., 2017; Hong et al., 2020; Luo & Lau, 2017; Park et al., 2012; Wang, Hui, et al., 2019; Wang, Jiang, et al., 2019 for China, Joshi et al., 2020; Ratnam et al., 2016; Rohini et al., 2016; Sandeep & Prasad, 2018 for India, Erdenebat & Sato, 2016 for Mongolia, Nishi et al., 2022; Noh et al., 2021 for Japan, Luo & Lao, 2018 for Indochina Peninsula). In RCP and SSP scenarios, the magnitude of daytime and nighttime Z500 anomaly against reference period climatology is much higher than the magnitude of that in Historical simulation, which may be one of the reasons for increase in CDNHWs (Figure S9 and Figure S10). The physical or dynamical mechanisms contributing to the increase in intensity and frequency of CDNHWs in each region of East Asia should be explored in-depth in further study.

In summary, the frequency and intensity of CDNHWs, which occur rarely during the heatwave periods in the present climate, will increase significantly by the end of the 21st century over the whole of East Asia. These increases are expected to be greater in Indochina, India, East China, and West China, compared to other regions.

AUTHOR CONTRIBUTIONS

Young-Hyun Kim: Writing – original draft; methodology; visualization; software; conceptualization; investigation; data curation; formal analysis; validation. **Joong-Bae Ahn:** Supervision; writing – review and editing; project administration; formal analysis. **Myoung-Seok Suh:** Data curation. **Dong-Hyun Cha:** Data curation. **Eun-Chul Chang:** Data curation. **Seung-Ki Min:** Data curation. **Young-Hwa Byun:** Data curation. **Jin-Uk Kim:** Data curation.

ACKNOWLEDGEMENTS

This work was carried out with the support of Cooperative Research Program for Agriculture Science and Technology Development (Project No. PJ01475503), Rural Development Administration, Republic of Korea.

ORCID

Young-Hyun Kim https://orcid.org/0000-0001-6046-3873
Joong-Bae Ahn https://orcid.org/0000-0001-6958-2801
Dong-Hyun Cha https://orcid.org/0000-0001-5053-6741
Seung-Ki Min https://orcid.org/0000-0002-6749-010X

REFERENCES

Ahsan, S., Bhat, M.S., Alam, A., Fqrooq, H. & Shiekh, H.A. (2022) Evaluating the impact of climate change on extreme temperature and precipitation events over the Kashmir Himalaya. *Climate Dynamics*, 58, 1651–1669. Available from: https://doi.org/10.1007/s00382-021-05984-6

Chen, W. & Dong, B. (2019) Anthropogenic impacts on recent decadal change in temperature extremes over China: relative roles of greenhouse gases and anthropogenic aerosols. *Climate Dynamics*, 52, 3643–3660. Available from: https://doi.org/10.1007/s00382-018-4342-9

Chen, Y. & Li, Y. (2017) An inter-comparison of three heat wave types in China during 1961-2010: observed basic features and linear trends. *Scientific Reports*, 7, 45619. Available from: https://doi.org/10.1038/srep45619

Choi, N. & Lee, M.-I. (2019) Spatial variability and long-term trend in the occurrence frequency of heatwave and tropical night in Korea. *Asia-Pacific Journal of Atmospheric Science*, 55, 101–114. Available from: https://doi.org/10.1007/s13143-018-00101-w

Ding, J., Cuo, L., Zhang, Y. & Zhu, F. (2018) Monthly and annual temperature extremes and their changes on the Tibetan Plateau and its surroundings during 1963-2015. *Scientific Reports*, 8, 11860. Available from: https://doi.org/10.1038/s41598-018-30320-0

Dong, S., Sun, Y., Aguilar, E., Zhang, X., Peterson, T.C., Song, L. et al. (2018) Observed changes in temperature extremes over Asia and their attribution. *Climate Dynamics*, 51(3), 339–353. Available from: https://doi.org/10.1007/s00382-017-3927-z

Erdenebat, E. & Sato, T. (2016) Recent increase in heat wave frequency around Mongolia: role of atmospheric forcing and possible influence of soil moisture deficit. *Atmospheric Science Letters*, 17(2), 135–140. Available from: https://doi.org/10.1002/asl.616

Fischer, E.M. & Schar, C. (2010) Consistent geographical patterns of changes in high-impact European heatwaves. *Nature Geoscience*, 3, 398–403. Available from: https://doi.org/10.1038/ngeo866

Freychet, N., Tett, S., Wang, J. & Hegerl, G. (2017) Summer heat waves over Eastern China: dynamical processes and trend attribution. *Environmental Research Letters*, 12, 024015. Available from: https://doi.org/10.1088/1748-9326/aa5ba3

Guo, J., Huang, G., Wang, X., Li, Y. & Lin, Q. (2018) Dynamically-downscaled projections of changes in temperature extremes over China. *Climate Dynamics*, 50, 1045–1066. Available from: https://doi.org/10.1007/s00382-017-3660-7

Hong, H., Sun, J. & Wang, H. (2020) Interdecadal variation in the frequency of extreme hot events in Northeast China and the possible mechanism. *Atmosphere Research*, 244, 105065. Available from: https://doi.org/10.1016/j.atmosres.2020.105065

Hong, J.-S., Yeh, S.-W. & Seo, K.-H. (2018) Diagnosing physical mechanisms leading to pure heat waves versus pure tropical nights over the Korean Peninsula. *JGR Atmospheres*, 123(14), 7149–7160. Available from: https://doi.org/10.1029/2018JD028360

Hu, T. & Sun, Y. (2020) Projected changes in extreme warm and cold temperatures in China from 1.5 to 5°C global warming. *International Journal of Climatology*, 40, 3942–3953. Available from: https://doi.org/10.1002/joc.6436

Im, E.-S., Choi, Y.-W. & Ahn, J.-B. (2017) Worsening of heat stress due to global warming I South Korea based on multi-RCM Ensemble projections. *JGR Atmosperes*, 122(1), 1444–11461. Available from: https://doi.org/10.1002/2017JD026731

Im, E.-S., Thanh, N.-X., Kim, Y.-H. & Ahn, J.-B. (2019) 2018 summer extreme temperatures in South Korea and their intensification under 3°C global warming. *Environmental Research Letters*, 14(9), 094020. Available from: https://doi.org/10.1088/1748-9326/ab3b8f

Joshi, M.K., Rai, A., Kulkarni, A. & Kucharski, F. (2020) Assessing changes in characteristics of hot extremes over India in a warming environment and their driving mechanisms. *Scientific Reports*, 10, 2631. Available from: https://doi.org/10.1038/s41598-020-59427-z

Kim, M.-K., Oh, J.-S., Park, C.-K., Min, S.-K., Boo, K.-O. & Kim, J.-H. (2019) Possible impact of the diabatic heating over the Indian subcontinent on heat waves in South Korea. *International Journal of Climatology*, 39(3), 1166–1180. Available from: https://doi.org/10.1002/joc.5869

Lee, W.-S. & Lee, M.-I. (2016) Interannual variability of heat waves in South Korea and their connection with large-scale atmospheric circulation patterns. *International Journal of Climatology*, 36, 4815–4830. Available from: https://doi.org/10.1002/joc.4671

Li, D., Zou, L. & Zhou, T. (2018) Extreme climate event changes in China in the 1.5 and 2°C warmer climates: results from statistical and dynamical downscaling. *JGR Atmosperes*, 123(18), 10215–10230. Available from: https://doi.org/10.1029/2018JD028835

Li, Y., Ding, Y. & Li, W. (2017) Observed trends in various aspects of compound heat waves across China from 1961 to 2015. *Journal of Meteorological Research*, 31, 455–467. Available from: https://doi.org/10.1007/s13351-017-6150-2

Li, Y., Ding, Y. & Liu, Y. (2021) Mechanisms for regional compound hot extremes in the mid-lower reaches of the Yangtze River. *International Journal of Climatology*, 41(2), 1292–1304. Available from: https://doi.org/10.1002/joc.6808

Luo, M. & Lao, N.-C. (2018) Synoptic characteristics, atmospheric controls, and long-term changes of heat waves over the Indochina Peninsula. *Climate Dynamics*, 51, 2707–2723. Available from: https://doi.org/10.1007/s00382-017-4038-6

Luo, M., Lao, N.-C. & Liu, Z. (2022) Different mechanisms for daytime, nighttime, and compound heatwaves in southern China. *Weather and Climate Extremes*, 36, 100449. Available from: https://doi.org/10.1016/j.wace.2022.100449

Luo, M. & Lau, N.-C. (2017) Heat waves in southern China: synoptic behavior, long-term change, and urbanization effects. *Journal of Climate*, 30(2), 703–720. Available from: https://doi.org/10.1175/JCLI-D-16-0269.1

Ma, F., Yuan, X., Wu, P. & Zeng, Z. (2022) A moderate mitigation can significantly delay the emergence of compound hot extremes. *JGR Atmosphere*, 127(2), e2021JD035427. Available from: https://doi.org/10.1029/2021JD035427

Mukherjee, S. & Mishra, V. (2018) A sixfold rise in concurrent day and night-time heatwaves in India under 2°C warming. *Scientific Reports*, 8, 16922. Available from: https://doi.org/10.1038/s41598-018-35348-w

Nishi, A., Kusaka, H. & Nakamura, S. (2022) Mesoscale and local-scale climatology of extreme temperature events in Niigata, Japan. *International Journal of Climatology*, 42, 9897–9908. Available from: https://doi.org/10.1002/joc.7870

Noh, E., Kim, J., Jun, S.-Y., Cha, D.-H., Park, M.-S., Kim, J.-H. et al. (2021) The role of the Pacific-Japan pattern in extreme heatwaves over Korea and Japan. *Geophysical Research Letters*, 48, e2021GL093990. Available from: https://doi.org/10.1029/2021GL093990

Opitz-Stapleton, S., Sabbag, L., Hawley, K., Tran, P., Hoang, L. & Nguyen, P.H. (2016) Heat index trends and climate change implications for occupational heat exposure in Da Nang, Vietnam. *Climate Service*, 2-3, 41–51. Available from: https://doi.org/10.1016/j.cliser.2016.08.001

Panda, D.K., Mishra, A., Kumar, A., Mandal, K.G., Thakur, A.K. & Srivastava, R.C. (2014) Spatiotemporal patterns in the mean and extreme temperature indices of India, 1971–2005. *International Journal of Climatology*, 34(13), 3585–3603. Available from: https://doi.org/10.1002/joc.3931

Park, J.-K., Lu, R., Li, C. & Kim, E.B. (2012) Interannual variation of tropical night frequency in Beijing and associated large-scale circulation background. *Advances in Atmospheric Sciences*, 29, 295–306. Available from: https://doi.org/10.1007/s00376-011-1141-1

Ratnam, J.V., Behera, S.K., Ratna, S.B., Rajeevan, M. & Yamagata, T. (2016) Anatomy of Indian heatwaves. *Scientific Reports*, 6, 24395. Available from: https://doi.org/10.1038/srep24395

Rohini, P., Rajeevan, M. & Srivastava, A. (2016) On the variability and increasing trends of heat waves over India. *Scientific Reports*, 6, 26153. Available from: https://doi.org/10.1038/srep26153

Russo, S., Sillmann, J. & Fischer, E.M. (2015) Top ten European heatwaves since 1950 and their occurrence in the coming decades. *Environmental Research Letters*, 10, 124003. Available from: https://doi.org/10.1088/1748-9326/10/12/124003

Sandeep, A. & Prasad, V.S. (2018) Intra-annual variability of heat wave episodes over the east coast of India. *International Journal of Climatology*, 38(S1), e617–e628. Available from: https://doi.org/10.1002/joc.5395

Seo, Y.-W., Ha, K.-J. & Park, T.-W. (2021) Feedback attribution to dry heatwaves over East Asia. *Environmental Research Letters*, 16, 064003. Available from: https://doi.org/10.1088/1748-9326/abf18f

Su, Q. & Dong, W. (2019) Projected near-term changes in three types of heat waves over China under RCP4.5. *Climate Dynamics*, 53, 3751–3769. Available from: https://doi.org/10.1007/s00382-019-04743-y

Teutschbein, C. & Seibert, J. (2012) Bias correction of regional climate model simulations for hydrological climate-change impact studies: review and evaluation of different methods. *Journal of Hydrology*, 456-457, 12–29. Available from: https://doi.org/10.1016/j.jhydrol.2012.05.052

Tong, S., Li, X., Zhang, J., Bao, Y., Bao, Y., Na, L. et al. (2019) Spatial and temporal variability in extreme temperature and precipitation events in Inner Mongolia (China) during 1960-2017. *Science of the Total Environment*, 649, 75–89. Available from: https://doi.org/10.1016/j.scitotenv.2018.08.262

Ullah, S., You, Q., Chen, D., Sachinra, D.A., AghaKouchak, A., Kang, S. et al. (2022) Future population exposure to daytime and nighttime heat waves in South Asia. *Earth's Futures*, 10, e2021EF002511. Available from: https://doi.org/10.1029/2021EF002511

Wang, J., Chen, Y., Liao, W., He, G., Tett, S.F.B., Yan, Z. et al. (2021) Anthropogenic emissions and urbanization increase risk of compound hot extremes in cities. *Nature Climate Change*, 11, 1084–1089. Available from: https://doi.org/10.1038/s41558-021-01196-2

Wang, J., Chen, Y., Tett, S.F.B., Yan, Z., Zhai, P., Feng, J. et al. (2020) Anthropogenically-driven increases in the risks of summertime compound hot extremes. *Nature Communications*, 11, 528. Available from: https://doi.org/10.1038/s41467-019-14233-8

Wang, J., Feng, J., Yan, Z. & Chen, Y. (2020) Future risks of unprecedented compound heat waves over three vast urban agglomerations in China. *Earth's Futures*, 8(12), e2020EF001716. Available from: https://doi.org/10.1029/2020EF001716

Wang, P., Hui, P., Xue, D. & Tang, J. (2019) Future projection of heat waves over China under global warming within the CORDEX-EA-II project. *Climate Dynamics*, 53, 957–973. Available from: https://doi.org/10.1007/s00382-019-04621-7

Wang, X., Jiang, D. & Lang, X. (2019) Extreme temperature and precipitation changes associated with four degree of global warming above pre-industrial levels. *International Journal of Climatology*, 39, 1822–1838. Available from: https://doi.org/10.1002/joc.5918

Wu, J., Han, Z., Xu, Y., Zhou, B. & Gao, X. (2020) Changes in extreme climate events in China under 1.5°C–4°C global warming targets: projections using an Ensemble of Regional Climate

Model Simulations. *JGR Atmospheres*, 125(2), e2019JD031057. Available from: https://doi.org/10.1029/2019JD031057

Yoon, D., Cha, D.-H., Lee, M.-I., Min, K.-H., Jun, S.-Y. & Choi, Y. (2021) Comparison of regional climate model performances for different types of heat waves over South Korea. *Journal of Climate*, 34, 2157–2174. Available from: https://doi.org/10.1175/JCLI-D-20-0422.1

Yoon, D., Cha, D.-H., Lee, M.-I., Min, K.-H., Kim, J., Jun, S.-Y. et al. (2020) Recent changes in heatwave characteristics over Korea. *Climate Dynamics*, 55(7–8), 1685–1696. Available from: https://doi.org/10.1007/s00382-020-05420-1

You, Q., Jiang, Z., Wang, D., Pepin, N. & Kang, S. (2018) Simulation of temperature extremes in the Tibetan Plateau from CMIP5 models and comparison with gridded observations. *Climate Dynamics*, 51, 355–369. Available from: https://doi.org/10.1007/s00382-017-3928-y

Zhang, Y., Mao, G., Chen, C., Lu, Z., Luo, Z. & Zhou, W. (2020) Population exposure to concurrent daytime and nighttime heatwaves in Huai River Basin, China. *Sustainable Cities and Society*, 61, 102309. Available from: https://doi.org/10.1016/j.scs.2020.102309

Zhu, J., Wang, S. & Fischer, E.M. (2021) Increased occurrence of day–night hot extremes in a warming climate. *Climate Dynamics*, 59, 1297–1307. Available from: https://doi.org/10.1007/s00382-021-06038-7

SUPPORTING INFORMATION

Additional supporting information can be found online in the Supporting Information section at the end of this article.

How to cite this article: Kim, Y.-H., Ahn, J.-B., Suh, M.-S., Cha, D.-H., Chang, E.-C., Min, S.-K., Byun, Y.-H., & Kim, J.-U. (2023). Concurrent daytime and nighttime heatwaves in the late 21st century over the CORDEX-East Asia phase 2 domain using multi-GCM and multi-RCM chains. *International Journal of Climatology*, *43*(10), 4687–4701. https://doi.org/10.1002/joc.8111